Supplementary Information

Engineering 2D spin networks by on-surface encapsulation of azafullerene radicals in nanotemplates

Gregor Kladnik[1,2§], Luca Schio[2§], Gregor Bavdek[2,3§], Yuri Tanuma[4], Marion van Midden Mavrič[4], Erik Zupanič[4], Bastien Anézo[4,5], Ioanna K. Sideri[6], Nikos Tagmatarchis[6], Jannis Volkmann[7,8], Hermann A. Wegner[7,8], Andrea Goldoni[9], Christopher P. Ewels[5], Alberto Morgante[2,10], Luca Floreano[2], Denis Arčon[1,4*] and Dean Cvetko[1,2,4*]

[1] Faculty of Mathematics and Physics, University of Ljubljana, Ljubljana, Slovenia.

[2] CNR-IOM, Istituto Officina dei Materiali, Basovizza Area Science Park, Trieste, Italy.

[3] Faculty of Education, University of Ljubljana, Ljubljana, Slovenia.

[4] Jožef Stefan Institute, Ljubljana, Slovenia.

[5] Institut des Matériaux de Nantes Jean Rouxel (IMN), UMR 6502 CNRS, Nantes University, Nantes, France.

[6] Theoretical and Physical Chemistry Institute, National Hellenic Research Foundation, Athens, Greece.

[7] Institute of Organic Chemistry, Justus Liebig University Giessen, Giessen, Germany.

[8] Center for Materials research (ZfM/LaMa), Justus Liebig University Giessen, Giessen, Germany.

[9] Elettra Sincrotrone Trieste S.C.p.A., Basovizza, Trieste, Italy.

[10] Physics department, University of Trieste, Trieste, Italy.

§ G.K., L.S. and G.B. contributed equally to this work.

* Corresponding authors: denis.arcon@ijs.si; dean.cvetko@fmf.uni-lj.si

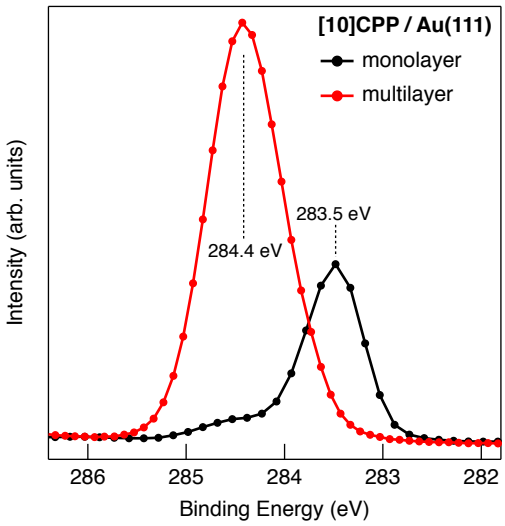

Figure S1. C1*s* XPS of [10]CPP deposited on Au(111). The main peak at 283.5 eV (black) corresponds to approximately 1 monolayer of [10]CPP, whereas for the multilayer we find the main peak at 284.4 eV (red). In the monolayer data the onset of the second layer (multilayer) C1*s* XPS signal can be seen as a shoulder at higher binding energy to the main peak.

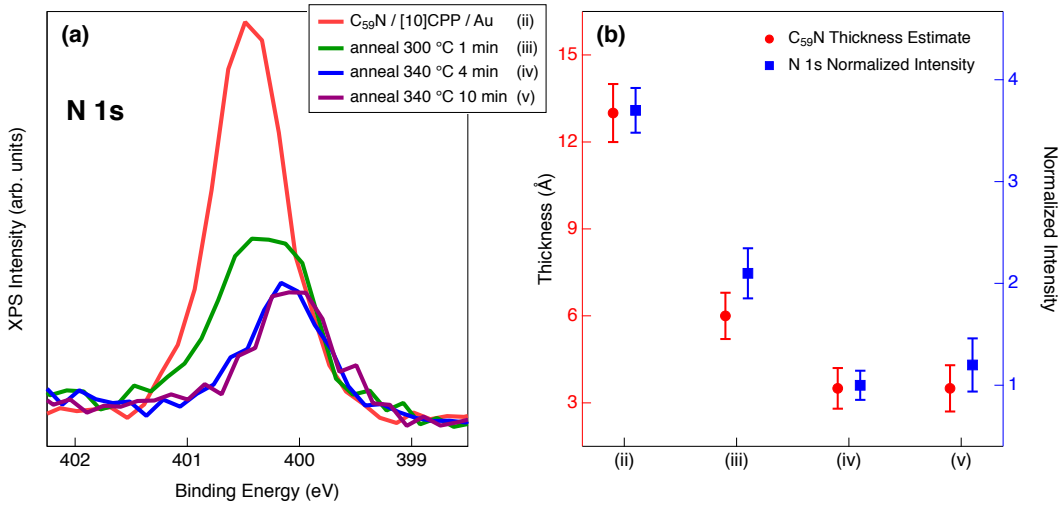

Figure S2: $C_{59}N$ Overlayer Thickness Estimate from XPS Data. (a) XPS N1*s* peak plotted for different steps during the annealing process: (ii) $C_{59}N$ as deposited on-top of [10]CPP on Au, (iii) annealing to 300 °C for 1 minute, (iv) additional annealing to 340 °C for 4 minutes and (v) further annealing to 340 °C for 10 minutes. The observed binding energy shift is consistent with weak substrate screening for multilayer (red) and stronger screening (blue) for monolayer coverages. (b) $C_{59}N$ thickness estimate (red) as deduced from the Au substrate signal attenuation (not shown) and the N1*s* normalized intensity (blue). Both indicate initial

desorption of the upper $C_{59}N$ layers in the multilayer (ii) - (iii), and stabilization of the $C_{59}N$ coverage at 340 °C (iv) - (v). The error bars are calculated from the N1*s* peak fit intensity uncertainty (data in blue) and the uncertainty of the electron attenuation length λ.

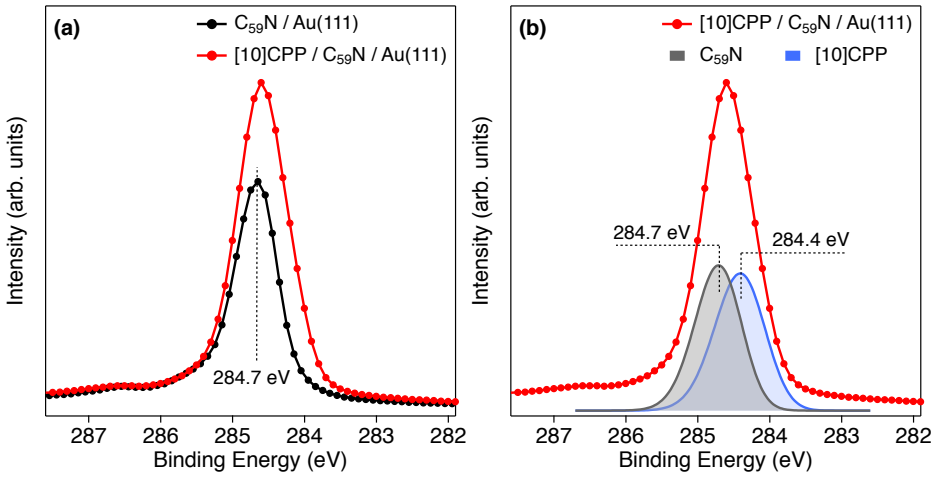

Figure S3. Comparison of C1*s* XPS of azafullerene on gold and with [10]CPP on-top. (a) C1*s* XPS of monolayer azafullerene $C_{59}N$ on Au(111) (black) at 284.7 eV binding energy (BE) and after depositing ~1 layer of [10]CPP on top (red). (b) decomposition of the C1*s* peak yields two components: first at 284.7 eV corresponding to $C_{59}N$/Au(111) (black), and second at 284.4 eV corresponding to the [10]CPP molecules atop (blue). Notice that the BE of the [10]CPP component matches the BE measured for the [10]CPP multilayer (Fig. S1) indicating that the [10]CPP molecules are not in direct contact with the Au substrate.

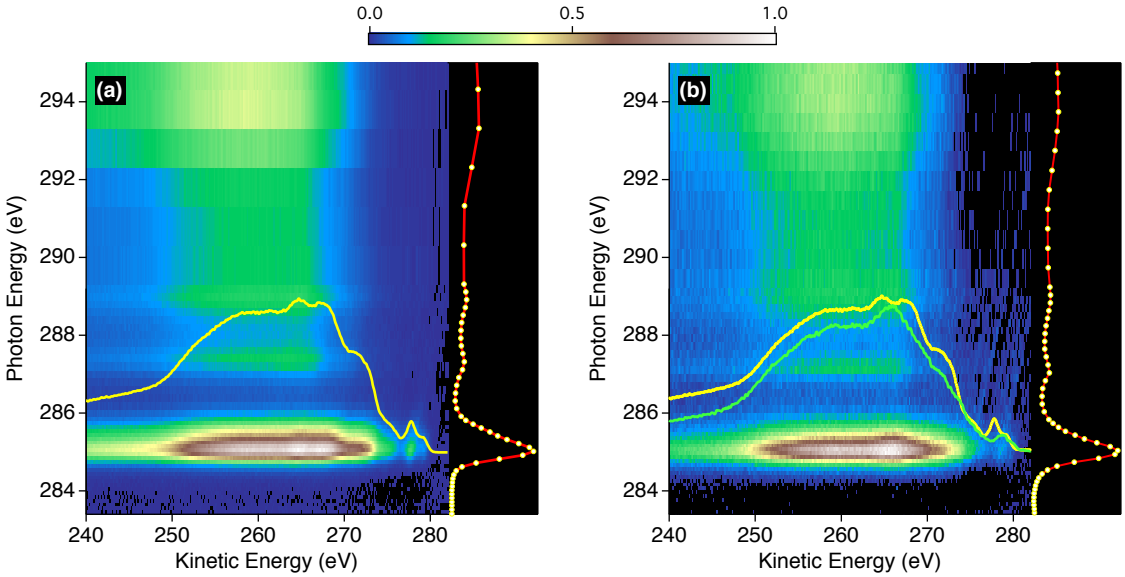

Figure S4. C K-edge resonant photoemission (RPES) of [10]CPP on Au(111). RPES data is represented as a 2D colour map of photoemission intensity in kinetic energy scale (horizontal axis) versus photon energy (vertical axis). To the right of each map the corresponding NEXAFS signal is shown. Single photoemission spectra taken at the resonance ($h\nu \approx 284.6$ eV) are shown as overlaid curves. (a) RPES of a multilayer which serves as a benchmark of participant Auger intensity. (b) RPES of a monolayer indicates quenched participant Auger intensity (yellow vs. green curve peaks) by a factor of 0.51 which translates into a charge transfer time of $\tau < 6$ fs (core-hole-clock method).

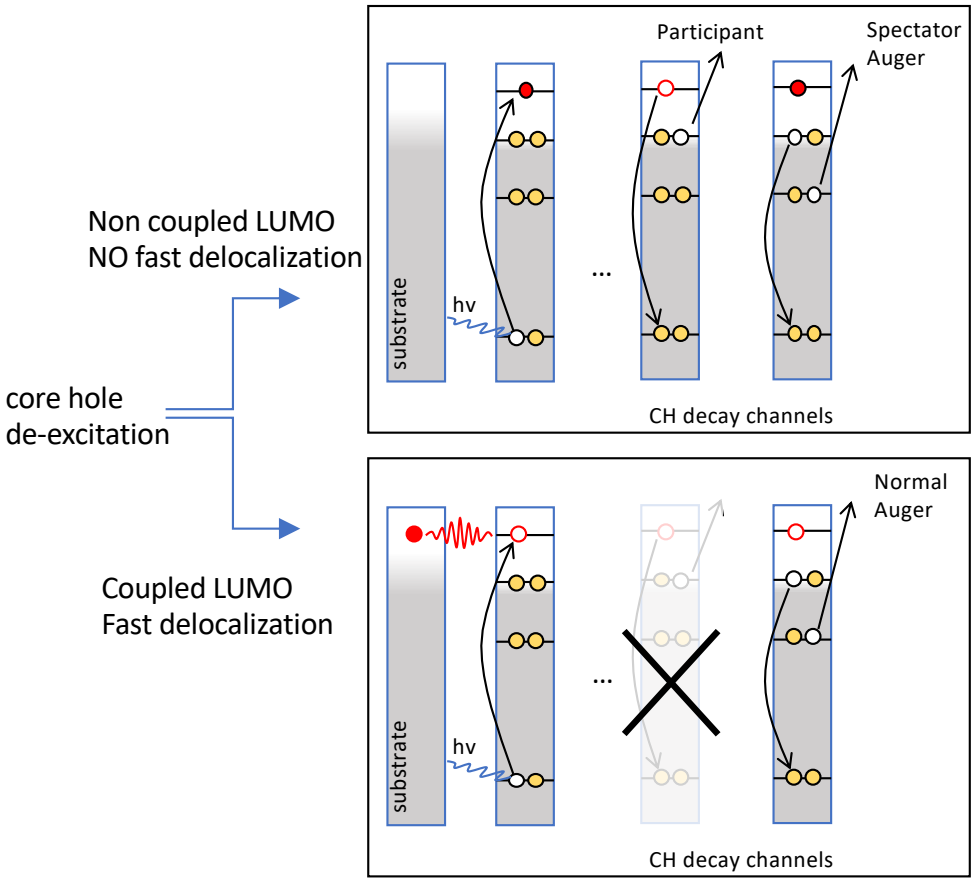

Figure S5. Principle of the RPES Core-Hole-Clock method. Following the creation of a core-hole (CH) by X-ray absorption the core-hole de-excitation occurs on the femtosecond timescale (τ_{ch}) with the emission of an Auger electron. Core-hole decay by "participant Auger" electron emission (upper panel) is energetically degenerate with direct photoelectron emission and in RPES spectra shows up as resonant increase of photoemission peaks at photon energies of resonant absorption (NEXAFS peaks). Core-hole de-excitation with the lowest unoccupied molecular orbital (LUMO) coupled to the substrate (bottom panel) leads to quenching of

Participant Auger emission (I_p<I_{p0}) due to ultrafast delocalization of the core excited electrons (red colour) from the site of excitation. Quantifying this quenching allows to determine the charge transfer time as $\tau_{CT} = \tau_{ch}\, I_p/(I_{p0}-I_p)$. Dark yellow filled circles represent electrons, empty (white) circles represent holes. The core-excited electron is shown as a red filled circle. Arrows indicate the different possible electron transitions.

Resonant photoemission – Auger spectator shift analysis

Nitrogen K-edge RPES intensity is presented in a 2D-like false colour map as a function of photon energy and electron kinetic energy (KE). Single electron emission scans measured at the N1*s*→LUMO resonance ($h\nu \approx 401.8$ eV) and off-resonance, above the vacuum continuum ($h\nu \approx 407$ eV) are shown in the lower panels as green and white colour curves, respectively. This latter, off-resonance spectrum, displays the Auger KVV emission line as a broad peak at ≈377 eV KE (indicated by vertical arrows in Fig.5).[1] For the on-resonance spectrum ($h\nu \approx 401.5$ eV) this Auger peak is found Coulomb shifted to higher kinetic energies due to the presence of the core excited electron in the LUMO during the core hole decay. This *spectator shift* (ΔE) of the Auger peak[2] at the N1*s*→LUMO resonance therefore correlates with the LUMO coupling and with the delocalization of the N1*s*→LUMO excited electron on the timescale of the core-hole decay[3]. We measure spectator shift $\Delta E \approx 2$ eV for the $C_{59}N^{\bullet}\subset$[10]CPP layer (Fig.5f) and almost no shift for the $(C_{59}N)_2$ dimerized layer, evidencing that N-based LUMO in the encapsulated radical assembly is effectively isolated and protected from coupling with the surface by the [10]CPP nanohoop. Lack of this protection in pristine $(C_{59}N)_2$ layers on Au(111) on the other hand results in increased coupling and delocalization of their N-based orbitals with almost negligible spectator shift of $\Delta E < 0.3$ eV. These values may be related to other organic systems with molecular coupling reflected in the measured Auger spectator shifts. For instance, in isolated fullerenes (C_{60}) with no charge transfer the spectator shift of 2-3 eV has been observed[2], whereas in coupled molecular systems with

amino-carboxylic bonding, orbital specific shifts of ~3.0 eV and ~1.7 eV have been observed at the C1*s*→LUMO and C1*s*→LUMO+1 resonance, respectively, corresponding to charge transfer times of >50 fs and <20 fs, respectively, reflecting the degree of LUMO and LUMO+1 orbital coupling involved in the intermolecular interaction[3].

Our N RPES measurements therefore show that [10]CPP encapsulation of azafullerene provides very efficient protection of N based orbitals on the $C_{59}N$ from electronic coupling with neighboring molecules and to the Au substrate. The protective shielding by the nanohoop evidently extends also on the neighboring carbon in the fullerene cage, where the singly occupied orbital of the $C_{59}N$ radical is mainly located. The [10]CPP encapsulation therefore provides valuable protection of the $C_{59}N$ radical against interaction and dimerization, which stabilizes the azafullerene's spin state on a long timescale.

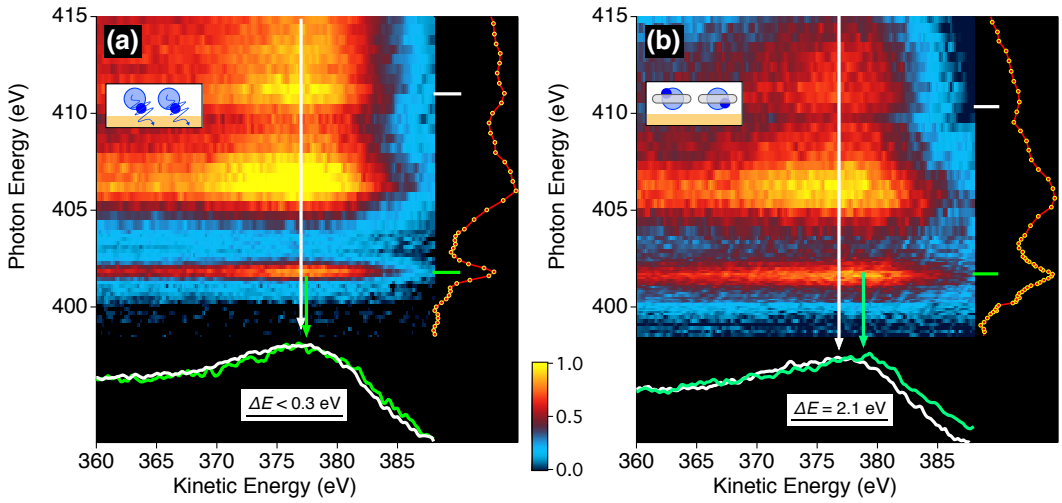

Figure S6. Nitrogen K-edge RPES of as-deposited and encapsulated azafullerenes. (a) Nitrogen K-edge RPES intensity map for the $(C_{59}N)_2$/Au(111) layer and (b) for the layer of $C_{59}N^{\bullet}\subset$[10]CPP assemblies shown in a 2D color map against photon energy (vertical axis) and electron kinetic energy (KE, horizontal axis). The broad electron emission peak is the N KVV Auger line peaked at ~ 377 eV KE (indicated by the vertical arrows). Single photoemission scans at the N1*s*→LUMO resonance ($h\nu = 401.3$ eV, green curve) and above the ionization edge ($h\nu \sim 407$ eV, white curve) are shown in the lower panels to evidence the KE »spectator« shift between the respective Auger peaks (ΔE). NEXAFS signal across the same photon energy

range is also shown aside on the top axis (yellow markers). Insets show cartoon representations of azafullerene (light blue circle with blue dot) and [10]CPP (grey ellipse) on gold substrate (dark yellow line).

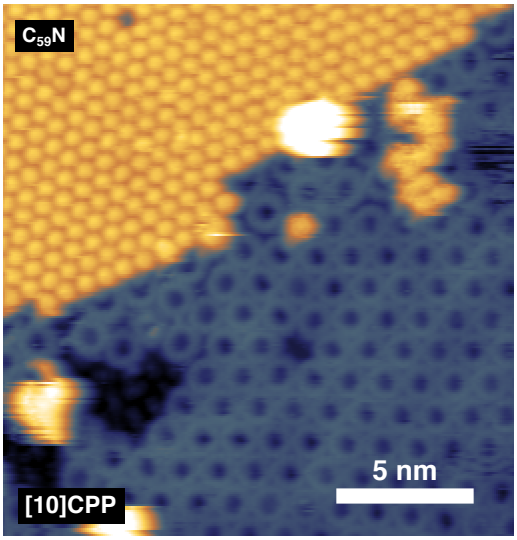

Figure S7. STM image of [10]CPP deposited on the $C_{59}N$/Au(111) sample at room temperature. The $C_{59}N$/Au(111) film was annealed to 320 °C prior to [10]CPP deposition. The image shows the coexistence of the $C_{59}N$/Au(111) and [10]CPP/Au(111) phases that prefer to form separate homogeneous islands. Sample bias U = -1.5 V, tunneling current I = -0.27 nA. The apparent height is represented by a false colour map (black-blue-yellow).

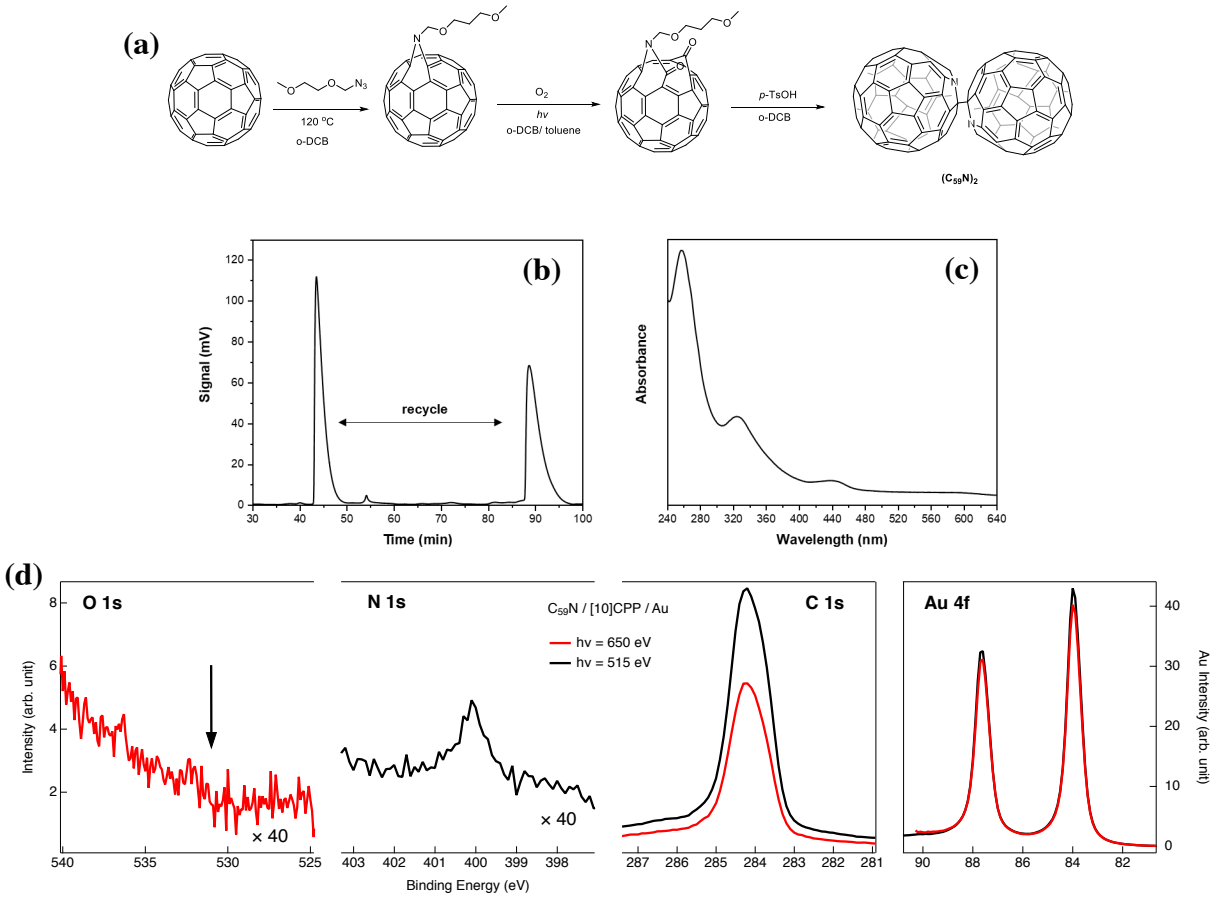

Figure S8. Synthesis, purification and XPS cleanness check of azafullerene. (a) Schematic presentation of synthesis and purification protocol for the parent $(C_{59}N)_2$ material. (b) Chromatograph of recycling preparative HPLC purification of $(C_{59}N)_2$ by using toluene as mobile phase, concentration of 1 mg/mL and flow rate of 8 mL/min. (c) UV-Vis spectrum of pure $(C_{59}N)_2$ in DCM. (d) XPS of $C_{59}N$/[10]CPP/Au layer taken at two different photon energies (515 eV and 650 eV) presented with black and red curves, respectively. Black arrow indicates the expected approximate binding energy of the O1*s* peak. The absence of any signal in this binding energy range proves that the prepared layer has no oxygen-related contamination.

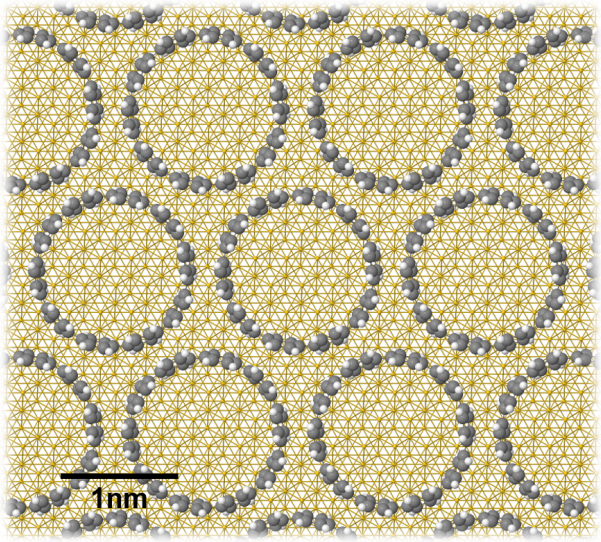

Figure S9. Structural optimisation of a layer of [10]CPP on Au(111). The optimisation yields a lattice parameter of $a_0 = 16.83$ Å. Grey spheres represent carbon atoms and white spheres hydrogen atoms of [10]CPP molecules. Dark yellow spheres represent gold atoms of the Au(111) substrate. See Methods section in main text for calculation details.

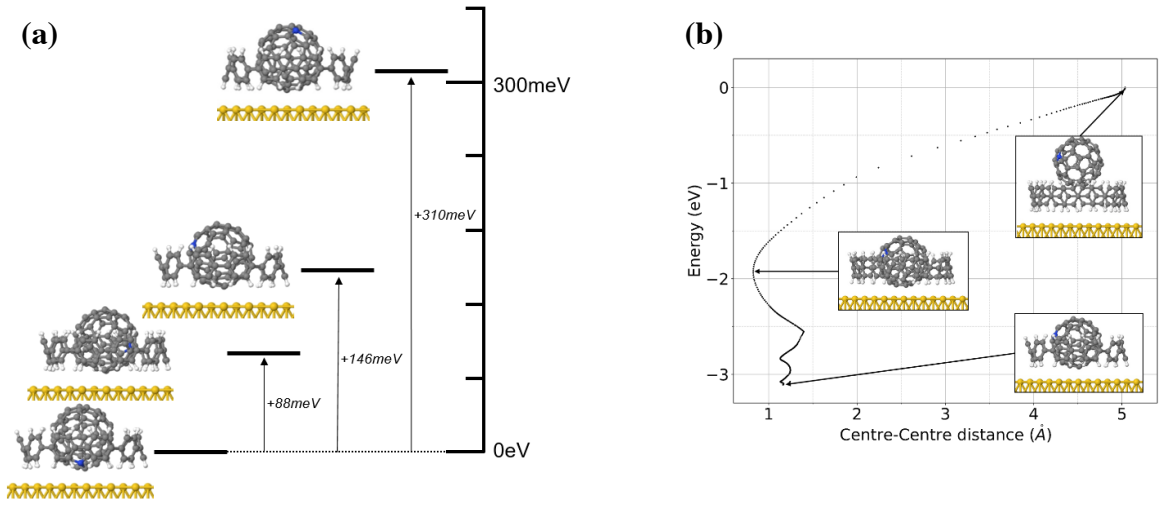

Figure S10: DFT geometry optimization of different $C_{59}N^{\bullet}\subset$[10]CPP supramolecular complexes on Au(111). (a) Several DFT geometry-optimized $C_{59}N^{\bullet}\subset$[10]CPP supramolecular complexes on Au(111) slab for different nitrogen (blue sphere) lone pair orientations and their relative energy scales. (b) Computed complexation energy for $C_{59}N^{\bullet}\subset$[10]CPP supramolecular complex on Au(111) as a function of the distance between the centers of host [10]CPP and guest $C_{59}N^{\bullet}$ radical. The lower section of this graph (from ~-2 to -3 eV) corresponds to rotations of the $C_{59}N^{\bullet}$ and [10]CPP, and reorganization of the CPP (change of dihedral angles, etc). The

complex and substrate are shown in ball and stick representation, with carbon atoms as grey balls, hydrogen atoms as white balls, the nitrogen atom as a blue ball and the gold atoms as yellow balls.

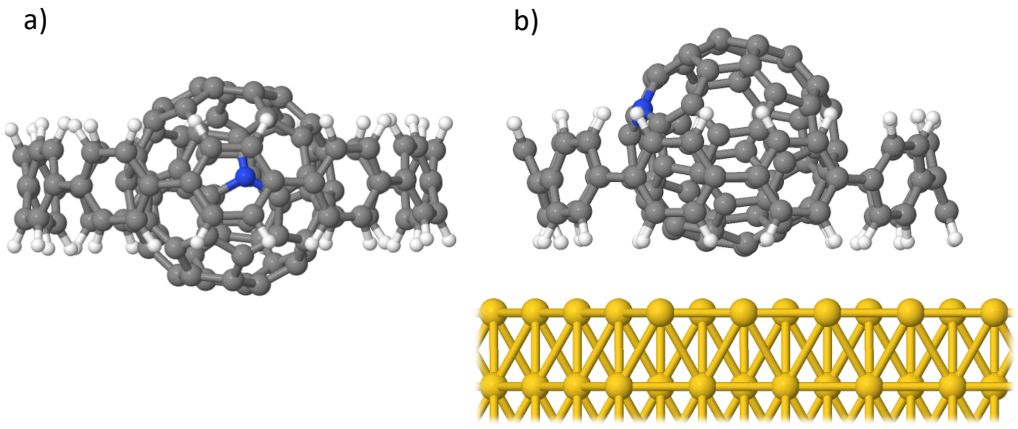

Figure S11: Ball and stick representation of the relaxed $C_{59}N^{\bullet}\subset$[10]CPP complex calculated by DFT. a) Gas phase and b) adsorbed on Au(111) surface. The blue ball represents the nitrogen atom in the azafullerene cage, grey balls represent carbon atoms, white balls hydrogen atoms and yellow balls the gold atoms. Animated complexation process of $C_{59}N^{\bullet}\subset$[10]CPP in the gas phase is shown in Supplementary Movie 1 in GIF format.

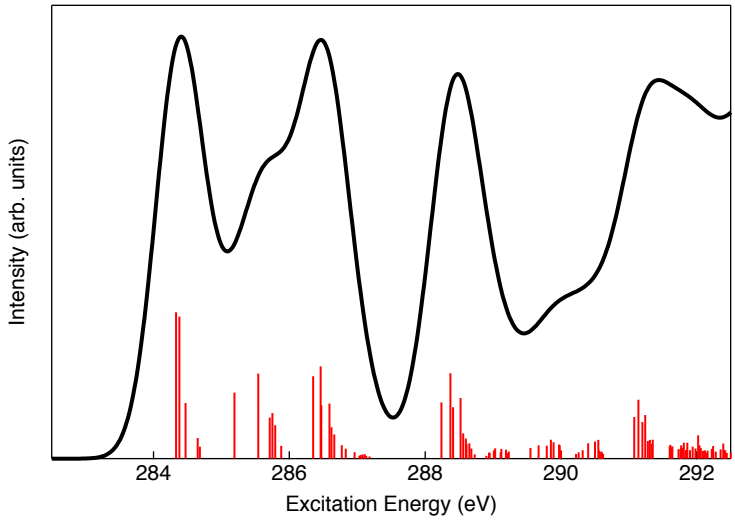

Figure S12. TD-DFT calculated C K-edge NEXAFS spectrum for $C_{59}N$. Red sticks indicate each NEXAFS excitation intensity and black curve shows the simulated spectrum obtained by Gaussian broadening (fwhm = 0.8 eV) the calculated transitions. The lowest energy transition peaks in the simulated spectrum at 284.5 eV, 286.5 eV and 288.5 eV reproduce nicely the measured NEXAFS features in Fig. 3a corroborating that the observed transitions belong to the $C_{59}N$ molecule. The calculated excitation energies are offset to match the observed lowest energy transition C1*s*→LUMO at 284.5 eV.

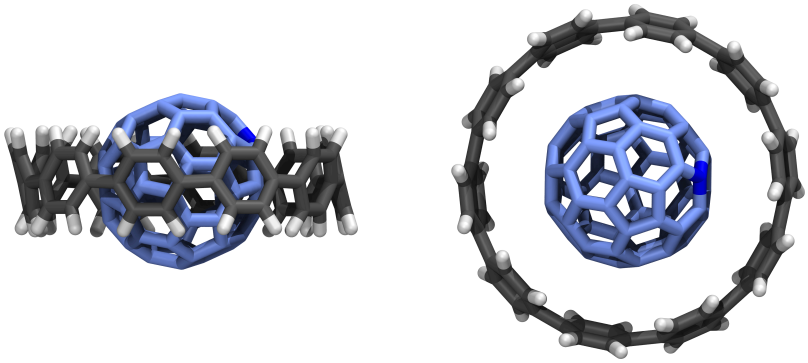

Figure S13. Stick representation of the DFT optimized geometry of the isolated $C_{59}N^{\bullet}$⊂[10]CPP complex. Sideview left, topview right. Carbon atoms in $C_{59}N^{\bullet}$ are coloured differently (light blue) than in [10]CPP (grey) for better representation of the complex. Distance between $C_{59}N^{\bullet}$ and [10]CPP is determined to be between ~3.4 Å – 3.7 Å, consistent with observations of the distances between fullerene C_{60} and [10]CPP.[4,5]

References

1. Ungier, L. & Thomas, T. D. Near threshold excitation of K V V Auger spectra in carbon monoxide using electron–electron coincidence spectroscopy. *J. Chem. Phys.* **82**, 3146–3151 (1985).
2. Brühwiler, P. A., Karis, O. & Mårtensson, N. Charge-transfer dynamics studied using resonant core spectroscopies. *Rev. Mod. Phys.* **74**, 703–740 (2002).
3. Kladnik, G. *et al*. Ultrafast Charge Transfer Pathways Through A Prototype Amino-Carboxylic Molecular Junction. *Nano Lett.* **16**, 1955–1959 (2016).
4. Xia, J., Bacon, J. W. & Jasti, R. Gram-scale synthesis and crystal structures of [8]- and

[10]CPP, and the solid-state structure of C60@[10]CPP. *Chem. Sci.* **3**, 3018 (2012).

5. Li, H. *et al*. Probing the deformation of [12]cycloparaphenylene molecular nanohoops adsorbed on metal surfaces by tip-enhanced Raman spectroscopy. *J. Chem. Phys.* **153**, (2020).